Journal of Building Engineering 57 (2022) 104830

Contents lists available at ScienceDirect

Journal of Building Engineering

journal homepage: www.elsevier.com/locate/jobe

Influence of strain rate on the mechanical properties of autoclaved aerated concrete

Ningombam Reena Devi [a], Prateek Kumar Dhir [b,*], Pradip Sarkar [a]

[a] Department of Civil Engineering, National Institute of Technology, Rourkela, Odisha, 769008, India
[b] Department of Civil and Environmental Engineering, University of Strathclyde, Glasgow, UK

ARTICLE INFO

Keywords:
Autoclaved aerated concrete
Strain rate
Compressive strength
Splitting tensile strength
Elastic modulus
Finite element method

ABSTRACT

The present work evaluates compressive strength and splitting tensile strength of Autoclaved Aerated Concrete (AAC) through systematic laboratory testing under varying strain rate conditions followed by a numerical calibration study. The result of this study shows that both the compressive and splitting tensile strength are significantly dependent on displacement rate. It was found that the compressive strength and the split tensile strength increase approximately 2.5 and 1.5 times respectively, while the elastic modulus increases approximately four times when the displacement rate increases from 0.1 mm/min at 10 mm/min. An empirical relationship is established using the experimental results to find the dynamic strength properties of AAC as a function of the static strength properties. The experimental outcomes of the present study are further calibrated using commercially available software called Abaqus, and numerical models are proposed to predict the expected strength of the AAC block at any level of strain rate.

1. Introduction

Autoclaved aerated concrete (AAC) has appeared as a possible alternative to the conventional clay and fly ash bricks [1–4] for the construction of infill masonry due to its various favorable properties like lighter weight, easier workability and workmanship, fire resistance, and thermal insulation capabilities. Infill walls have a significant contribution towards the overall strength and stiffness of the framed buildings especially under lateral dynamic loading. Compressive strength, elastic modulus, and the stress-strain relationship of AAC block under dynamic load influence the safety and reliability of AAC block infilled framed buildings. Masonry walls are expected to undergo a very high displacement rate during stormwinds and earthquakes. During the analysis and design of a structure, the peak loads are applied either statically or dynamically, and the appropriate resistance provided by the structural system needs to be determined. To calculate the resistance of the structure, the constitutive properties of AAC over a wide range of strain rates are required. Therefore, the understanding of the behavior of AAC blocks under different strain rates is of considerable importance. Most of the past studies [1,2,5] have evaluated different mechanical properties of AAC block considering a constant loading rate (approximately in the range of 0.5–2.0 mm/min). A detailed literature review revealed that there are no specific studies available on the effect of loading rate on the AAC block or its masonry. Małyszko et al. [5] carried out the splitting tensile strength tests and simulated the failure mechanism. Some experiments [1,2] have been performed, but still, no physical mechanism can clearly explain the strain rate effect for AAC. So, the primary objective of the present paper is to investigate the effect of strain rate on compressive strength and splitting tensile strength of AAC under monotonic compressive loading which can quantitatively explain the strain rate

* Corresponding author.
E-mail addresses: reena.ning@gmail.com (N.R. Devi), prateek.dhir@strath.ac.uk (P.K. Dhir), sarkarp@nitrkl.ac.in (P. Sarkar).

https://doi.org/10.1016/j.jobe.2022.104830
Received 30 January 2022; Received in revised form 30 May 2022; Accepted 14 June 2022
Available online 21 June 2022

effect for AAC under high (1.0–10.0 mm/min), medium (1.0 mm/min) and low (0.1–1.0 mm/min) strain rates. The purpose of this study is to help improve the knowledge of the mechanical properties of AAC by studying the rate-sensitive response of its constituents. Limited studies are available on the mechanical properties of AAC blocks [1–5] and no study is available that proposes the modelling strategy to estimate the mechanical properties numerically. In this paper, the failure behaviors of individual AAC blocks during the test are discussed. Thus, the present article studies the comprehensive mechanical behavior of AAC.

However, the previous literature reports several experimental studies on the importance of displacement rates in determining the compressive strength of other brittle materials such as concrete, clay bricks, and cement mortars. Harsh et al. [6] studied the strain-rate sensitivity of the cement paste and mortar constituents of concrete experimentally and observed that the strain at the maximum stress is the greatest for the lowest strain rate. With an increase in strain rate, the strain at the maximum stress first decreases and then increases. Wang et al. [7] conducted an extensive experiment to investigate the compressive behavior of cement-asphalt mortar when the temperature and loading rate are changed. Yao et al. [8] evaluated the mechanical properties of alkali-activated binder-based mortars subjected to dynamic loading and found that the dynamic compressive and tensile strengths of alkali-activated mortars increase with the loading rates. Experimental results [9,10] indicate that the strain rate has a significant influence on the compressive strength of the clay brick and mortar. Previous studies [11–14] have demonstrated that most materials, in general, show an increase in strength as the loading rate increases. Hao and Zhou [15] reported that the uniaxial tensile strength of concrete increases by approximately seven to eight times of its static strength at the strain rate of 200/s, while the uniaxial compressive strength increases by two to three times at the same strain rate. Table 1 represents the previous studies conducted on the displacement/strain/load rates on various brittle materials.

A numerical model calibration study was performed using a commercially available finite element software called Abaqus [16] to estimate the strain rate effect on masonry units based on the homogenisation theory. A typical unit masonry is selected to serve as a representative volume element (RVE). Numerical models of the RVE are established with detailed distinctive modelling of brick with its dynamic material properties obtained from laboratory tests. Monotonic compressive loads of different loading rates are considered and a continuum damage model accounting for the strain rate effect is then developed for the unit masonry. The scale effect of the RVE, as well as the reliability of the homogenised masonry material model, is also numerically verified. The research methodology adopted in this study is outlined in Fig. 1 in the form of a flow chart.

AAC is an emerging masonry material that requires comprehensive research outputs to be accepted as an alternative to conventional masonry materials and to support structural design. Consequently, considerable research effort has been made in this direction, as is apparent from the published literature. However, the effect of strain rate on the stress-strain behavior of AAC has not received any research attention until now. This article addresses the above research gap by conducting an experimental program to study the effect of strain rate under monotonic compression, as well as tension under low, medium, and high load rates. Also, the present article demonstrates a numerical modeling strategy to study the mechanical behavior of AAC and the associated failure behaviors under various load rates.

Table 1
Previous studies of brittle materials on the varying strain rate.

Literature	Displacement/strain rate	Material	Mechanical properties tested
Raj et al., 2020 [1]	0.01 mm/s	AAC	Compressive strength; shear and tensile bond strength
Bhosale et al., 2019 [2]	1 mm/min	AAC	Compressive strength; shear and tensile bond strength
Małyszko et al., 2017 [5]	0.5 mm/min	AAC	Splitting tensile strength of cube specimen
Małyszko et al., 2017 [5]	2.0 mm/min	AAC	Splitting tensile strength of cylindrical specimen
Bhosale et al., 2020 [17]	1 mm/min	CLC	Compressive strength; shear and tensile bond strength
Barattucci et al., 2020 [18]	0.05, 0.10, 1 mm/min	Clay brick masonry; masonry mortar	Flexural, compressive and shear strength
Hao and Tarasov, 2008 [9]	0.001, 1, 10, 50, and 200 s^{-1}	Clay brick and cement mortar	Compressive strength
Kaushik et al., 2007 [19]	–	Clay brick and cement mortar	Compressive Strength
Feng et al., 2015 [12]	10^{-6}, 10^{-5} and 10^{-4} s^{-1}	Geopolymer concrete and mortar	Compressive Strength
Khandelwal et al., 2013 [13]	0.001, 0.005, 0.01 and 0.05 mm/s	Geopolymer mortar	Compressive strength
Reis et al., 2014 [20]	0.05, 0.1, 0.5, 5, 50, and 100 mm/min	Polymer mortar	Flexural strength
Wang et al., 2016 [7]	1, 5, 10, 20, 30, 40 and 50 mm/min	Cement asphalt mortar	Compressive strength
Wang et al., 2015 [21]	0.001, 0.003, 0.005, 0.007, and 0.009 min^{-1}	Cement asphalt mortar	Compressive strength
Zhang et al., 2020 [22]	5.0×10^{-4}, 5.0×10^{-1}, and 1.6×10^{1} mm/s	Cement mortar	Flexural and compressive strengths
Ranjith et al., 2008 [14]	0.05, 0.10, 0.15, 0.20, and 0.25 mm/min	Concrete	Compressive strength
Tandon and Faber, 1999 [23]	0.25, 1, 10, and 100 μm/min	Cement paste, mortar, and concrete	Compressive strength
Oh, 1990 [24]	0.8333×10^{-3} (static) to 0.8333 (dynamic) mm/s	Concrete	Flexural strength

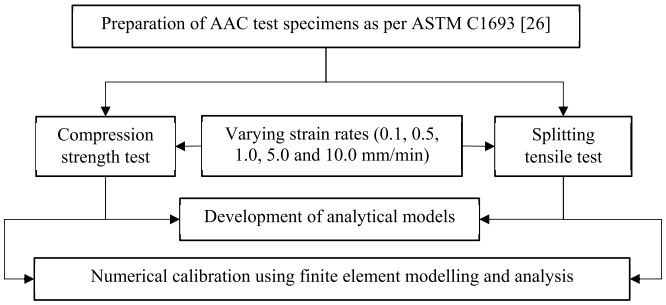

Fig. 1. The research methodology adopted in this study.

2. Experimental campaign

Commercially available AAC blocks conforming to Class-III of Indian Standard [25] with an actual size of 600 × 200 × 100 mm^3 as shown in Fig. 2a were collected. A total of 60 cubic specimens of edge length 100 mm (Fig. 2b) were cut from AAC blocks using a diamond blade cutter and AAC hacksaw to evaluate the compressive and splitting-tensile strength as per ASTM [26]. The information regarding the position of the cubes and rise was also reported (Fig. 3). Load bearing surfaces of the specimen were kept plane within 0.0035 inches (0.09 mm) per 4.0 inches (100 mm) which were achieved by grinding, milling, or capping. The scope of the present study was kept limited to evaluate the effect of strain rate on the strength of the AAC specimens. Therefore, all the AAC specimens used in the present study are taken from the same batch to avoid the variations arising out of a change in their physical properties. Detailed physical properties of each of the AAC samples were tested prior to performing the strength tests, the results of which are presented in Table 2. However, further investigations to quantify the influence of these physical properties on AAC strength properties are not considered within the scope of the present study. The cube specimens were tested in a displacement-controlled universal testing machine (Instron SATEC with a maximum load capacity of 600 kN) to determine its stress-strain behavior under monotonic compressive and splitting-tensile load.

2.1. Compression test

The compression tests were performed in accordance with ASTM [26]. The compressive strength of AAC cube units depends on the specimen size and shape, method of pore formation, the direction of loading, age, and characteristics of ingredients used [28–37]. In the present study, a total of 30 AAC cube specimens of size 100 mm were prepared and a set of 6 samples were tested perpendicular to the direction of rise [26] under uniaxial monotonic compressive loading for each of the five selected strain rates. Following five specific strain rates were selected for this study based on the discussion presented in the Introduction section: 0.1, 0.5, 1.0, 5.0, and 10.0 mm/min.

Before placing the cube specimens at the compression testing machine, specifications such as mass, dimension, and the direction of the rise of each specimen were recorded. After they were checked, specimens were carefully positioned at the centre of the compression testing machine, to prevent possible unsatisfactory failures of cube specimens. Fig. 4a shows a typical AAC cube specimen positioned in the compression testing machine while Fig. 4b presents a typical specimen that failed after the compression test.

The uniaxial stress-strain curves obtained from the compression tests are presented in Fig. 5. The experimental results indicate that

Fig. 2. AAC blocks (a) as procured and (b) cube specimens used for the experiments.

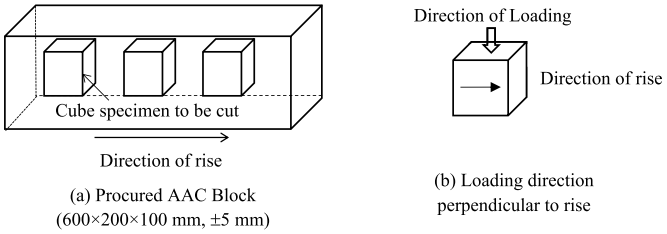

(a) Procured AAC Block (600×200×100 mm, ±5 mm)

(b) Loading direction perpendicular to rise

Fig. 3. Direction of loading for compression test and splitting-tensile test of cube specimen.

Table 2
Physical properties of the AAC samples tested and the test conditions.

Properties	Standards	Mean Value[a]
Bulk density (kg/m^3)	ASTM C1693 [26]	611 (0.06)
Moisture content (%)	ASTM C1693 [26]	14.54 (0.26)
Initial Rate of Absorption (kg/m^2/min)	ASTM C67 [27]	1.70 (0.17)
Atmospheric Temperature (°C)	–	24.6
Relative Humidity (%)	–	50–70

[a] The values in parentheses indicate the coefficient of variation.

Fig. 4. (a) Test setup for determining the compressive strength and (b) Typical failure mode after compressive test of the AAC cube unit.

the stress-strain curve, peak stress, corresponding axial strain, and the elastic modulus of AAC cube specimens are affected by the increase of the loading rate. Fig. 5 shows that the compressive strength and elastic modulus of AAC specimen increase with the increase of loading rate. Previous studies [11–13] have shown that most materials demonstrate increases in strength and stiffness as the loading rate or strain rate increases. The range of values of compressive strength and elastic modulus of AAC specimen evaluated experimentally agree with several past studies [1,13,38]. It is to be noted that the density and elastic modulus of AAC block is significantly lower than that of conventionally used masonry materials such as clay and fly ash bricks. Such low value of density and elastic modulus encourages the usage of AAC block in the infill masonry construction at seismic prone areas [1,39].

The codes and standards do not specify any satisfactory failure pattern for AAC cube specimens under uniaxial compression loading. However, European standards [40] recommend satisfactory and unsatisfactory failure patterns for cube specimens of another brittle material (concrete) under uniaxial compression loading. The failure modes observed in the present compression test of AAC block are evaluated in light of the recommendations of European standards [40]. Fig. 6 summarised different actual failure modes observed in the cube specimens during the compression test of AAC block specimens for varying displacement rates. It has been observed that the four exposed sides of AAC specimens were cracking uniformly at the peak load for all the displacement rates, while the top and bottom sides remained with small or no cracking and damages. It can also be seen that the most common type of failure

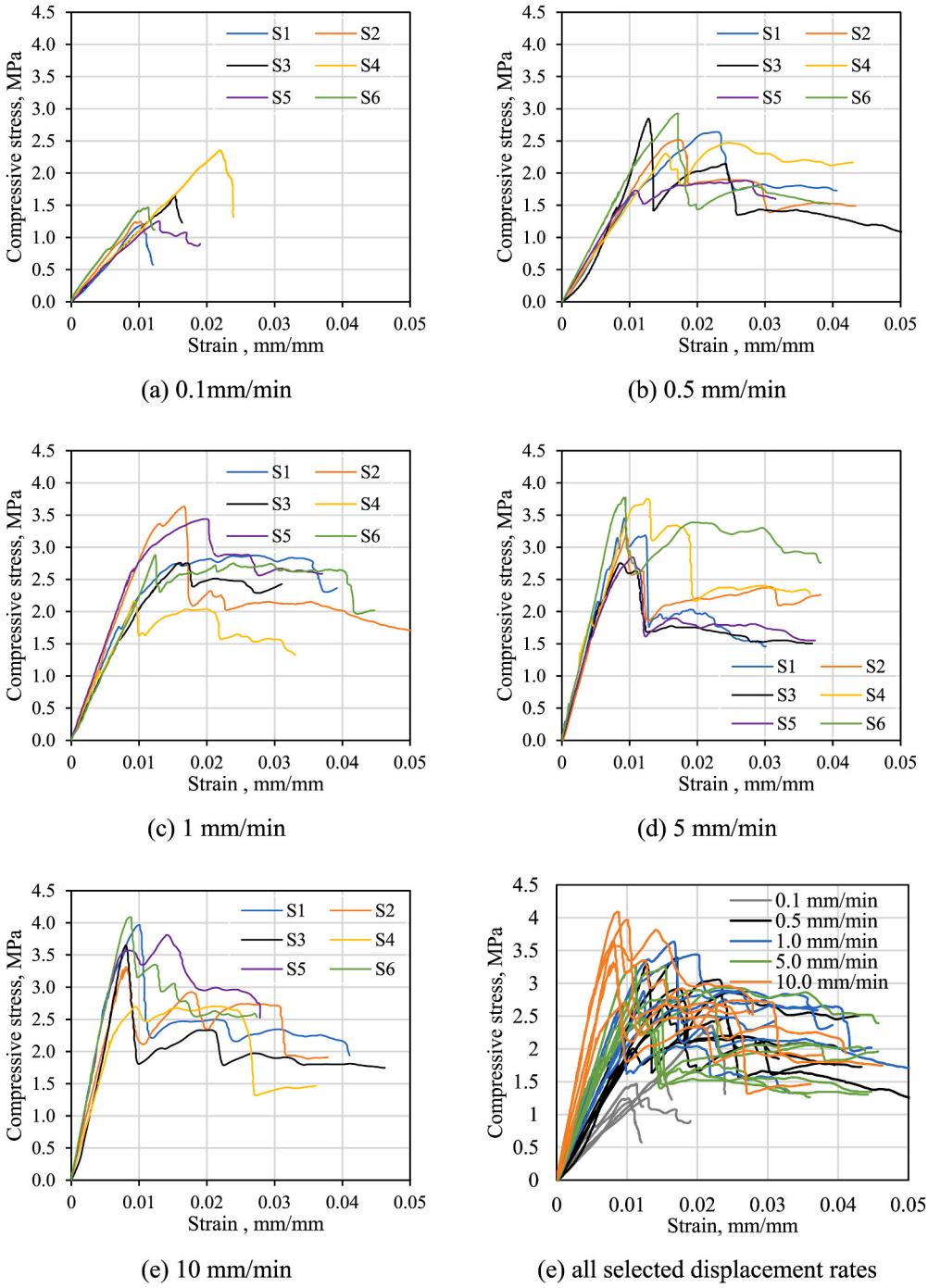

Fig. 5. Comparison of uniaxial compression responses of AAC cubes.

pattern observed has the cracking at approximately 45° (two truncated pyramids, one inverted over the other) to the axis near the ends of cube specimens as shown in Fig. 4b. The fine cracks appeared parallel to the loading direction on all side surfaces at first. When the peak stress was approached, these vertical cracks linked together and developed into larger cracks, which tended to separate the AAC cube into slender columns. In the end, the AAC cube essentially failed by buckling in all four sides. Such a pattern of failure conforms to the failure modes outlined in the past studies and standard code [2,40]. This result indicates that loading rates do not affect the modes of failure in the AAC cube specimens subjected to uniaxial compression load.

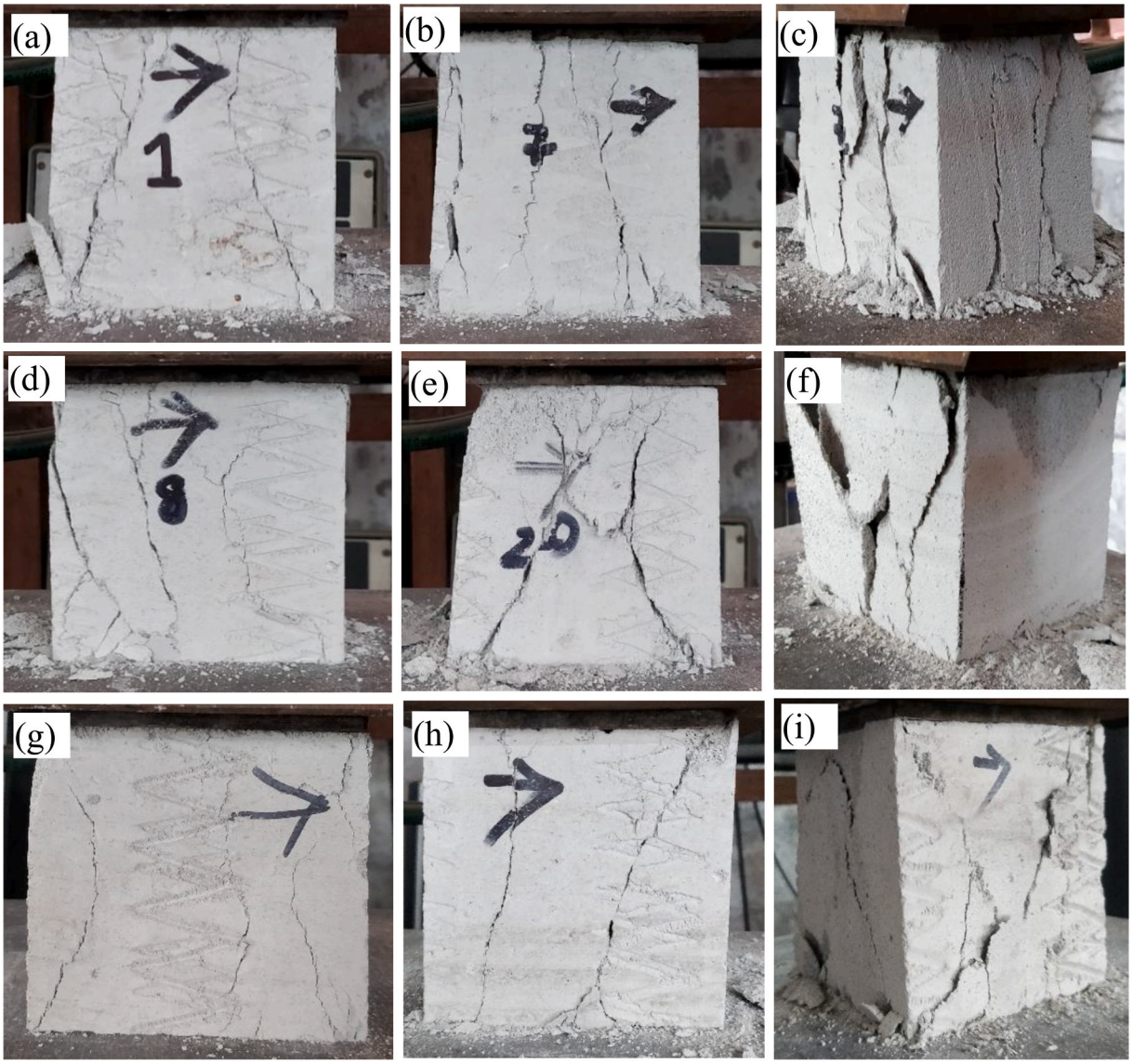

Fig. 6. Failure patterns observed in AAC cubes under uniaxial compression.

2.2. Splitting-tensile test

Although the most important structural characteristics of AAC are the compressive strength and the dry density, the mechanical behavior of structures made of AAC is also influenced by its little resistance to tensile stresses. Apart from cracks resulting from axial restraint to shrinkage and thermal movements, various forms of tensile cracking can occur. The resistance to tensile cracks in brittle materials, such as concrete, masonry units, rocks, or building ceramics, requires the knowledge of its tensile strengths. The split-tension is performed by placing a cube specimen between the platens of the test machine while the load is subsequently applied to failure. The splitting tension test has been performed on AAC cube specimens of 100 mm size applying compression load perpendicular to its base plane as per the recommendation of published literature [5]. The specimens were loaded through the plywood strips with 20 mm width, 3–4 mm thick, and a length not less than the side length of the specimen. The strips were placed in the middle of the upper and lower base plane of the specimens prior to tests. The load has been applied to the test specimen by vertical forces until a failure with various strain rates (0.1, 0.5, 1.0, 5.0, and 10 mm/min) using a displacement-controlled universal testing machine with a capacity of 600 kN as shown in Fig. 7.

The nominal splitting tensile strength (f_{st}) is calculated for the load at the failure (P) based on the elastic tensile stress theory as follows:

$$f_{st} = \frac{2P}{\pi A} \tag{1}$$

Fig. 7. (a) test setup for the split tensile test (b) AAC samples after the split tensile test.

where A = area of the splitting surface. Fig. 8 represents the splitting tensile stress versus axial strain curve of AAC cube specimens. It is observed that displacement rates have a large influence on the stress-strain curve, stiffness, and splitting tensile strength of AAC cube specimens. The splitting tensile strength of AAC cube specimens was found to be increasing with the increase of displacement or loading rate.

It is observed that the failure of the AAC cube specimen starts in the contact zone near the plywood strips leading to a central vertical crack parallel to the loading and split into approximately two equal halves as shown in Fig. 9. Similar nature of the failure pattern in splitting tensile test of AAC and concrete specimens was also reported in the previous literature [5,41]. Fig. 8 shows that the loading rate has no significant influence on the results of the splitting failure pattern. However, cracks in the high loading rate expanded quickly once they occurred and even burst when the specimens were damaged, showing a typical brittle failure. Higher rates of loading were quick splitting cracks, making the specimen exhibit a typical brittle failure.

2.3. Regression analysis

Key parameters such as compressive strength, strain at peak compressive stress, modulus of elasticity, and splitting tensile strength were evaluated from Figs. 5 and 8 are presented in Table A1 (in Appendix A) for all individual specimens tested. The compressive strength was calculated corresponding to the peak load of failure as per ASTM [26]. The chord modulus of elasticity was taken between 5% and 33% of the maximum compressive strength of each cube specimen. The average results for each of the selected displacement rates are summarised in Table 3. Table 3 also present the expanded uncertainty calculated considering a 95% confidence interval [42]. It should be noted here that the outlying observations of the experiment results have been eliminated as per Indian Standard IS:8900 [43] considering 5% level of significance before using them in the regression analysis. This table shows that all strength properties (compressive strength, split tensile strength, and elastic modulus) increase with increasing displacement rate. It can be seen from this table that the maximum compressive and splitting tensile strength are 3.59 MPa and 0.59 MPa respectively, at 10 mm/min strain rate, whereas the minimum compressive and splitting strengths are 1.53 MPa and 0.39 MPa at 0.1 mm/min strain rate. The strains at peak stress are found to be in the range of 0.0201 to 0.0098. The mean values of the splitting tensile strengths are in the typical range of 15–28% of the compressive strength. Table 4 compares the mean mechanical strength parameters (compressive and splitting tensile strength) of AAC cubes obtained experimentally in the present study with the results of existing literature. At a displacement rate of 0.5 mm/min, the compressive strength was found to be 2.54 MPa which is appx. 19% higher than the strength obtained by Raj et al. [1]. Whereas, at a displacement rate of 1.0 mm/min, the compressive strength (2.97 MPa) is quite close to the result obtained by Bhosale et al. [2]. Similarly, a mean Splitting Tensile Strength of 0.45 MPa was obtained at a displacement rate of 0.5 mm/min, which is 24% higher than the results obtained by Małyszko et al. [5] at the same level of displacement rate.

A change in the strain rate causes different behavior related to the mechanical properties of AAC. The strain at peak compressive stress, modulus of elasticity, compressive strength, and splitting tensile strength of the AAC specimen for various displacement rates relative to that of the slowest displacement rate (0.1 mm/min) are plotted in Fig. 10 against different displacement rates. Fig. 10 shows that when the displacement rate increases from 0.1 mm/min to 1.0 mm/min all the mechanical properties of AAC are found to increase significantly. To further increase of displacement rate, all the mechanical properties (except strain at peak stress) are found to be increasing although with a milder slope. This result shows the strength dependence of AAC on the displacement rate. Strength properties were found to increase slowly with increasing displacement rate, as indicated by the gentler slopes because the displacement rate range used in the study is lower. Similar behaviour was observed for many other brittle materials [44,45]. The dependence of AAC strength properties on the displacement rate is related to the thermo-activated mechanism and macro-viscous mechanism [44] that control the deformation and fracture of AAC. However, this aspect could not be studied in detail.

This distinct relation of compressive strength, elastic modulus, and splitting tensile strength with the load rate encouraged to develop a model that can predict these mechanical properties of the AAC cube as a function of the load rate. The general form of the considered model is presented as follows:

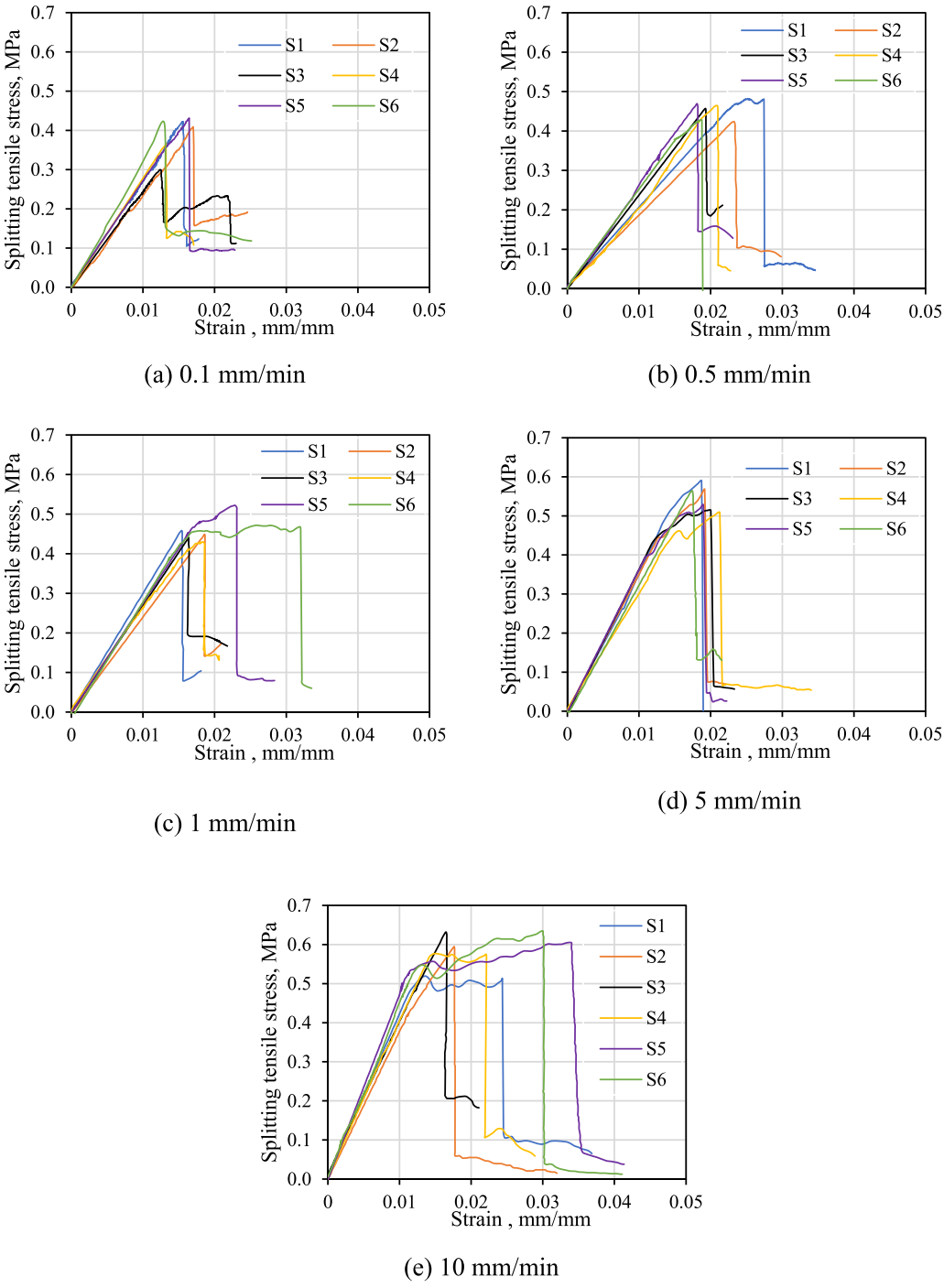

Fig. 8. Comparisons of split tensile response of AAC cubes.

$$x = x_0 + K \times \ln\left(\frac{R}{R_0}\right) \tag{2}$$

Where, 'x' is any of the three mechanical properties considered (i.e., compressive strength, elastic modulus, and tensile strength) under a given load rate (R). 'x_0' is the same property under static load rate, R_0 (considered here as 0.1 mm/min). K is a constant obtained through regression analysis as follows:

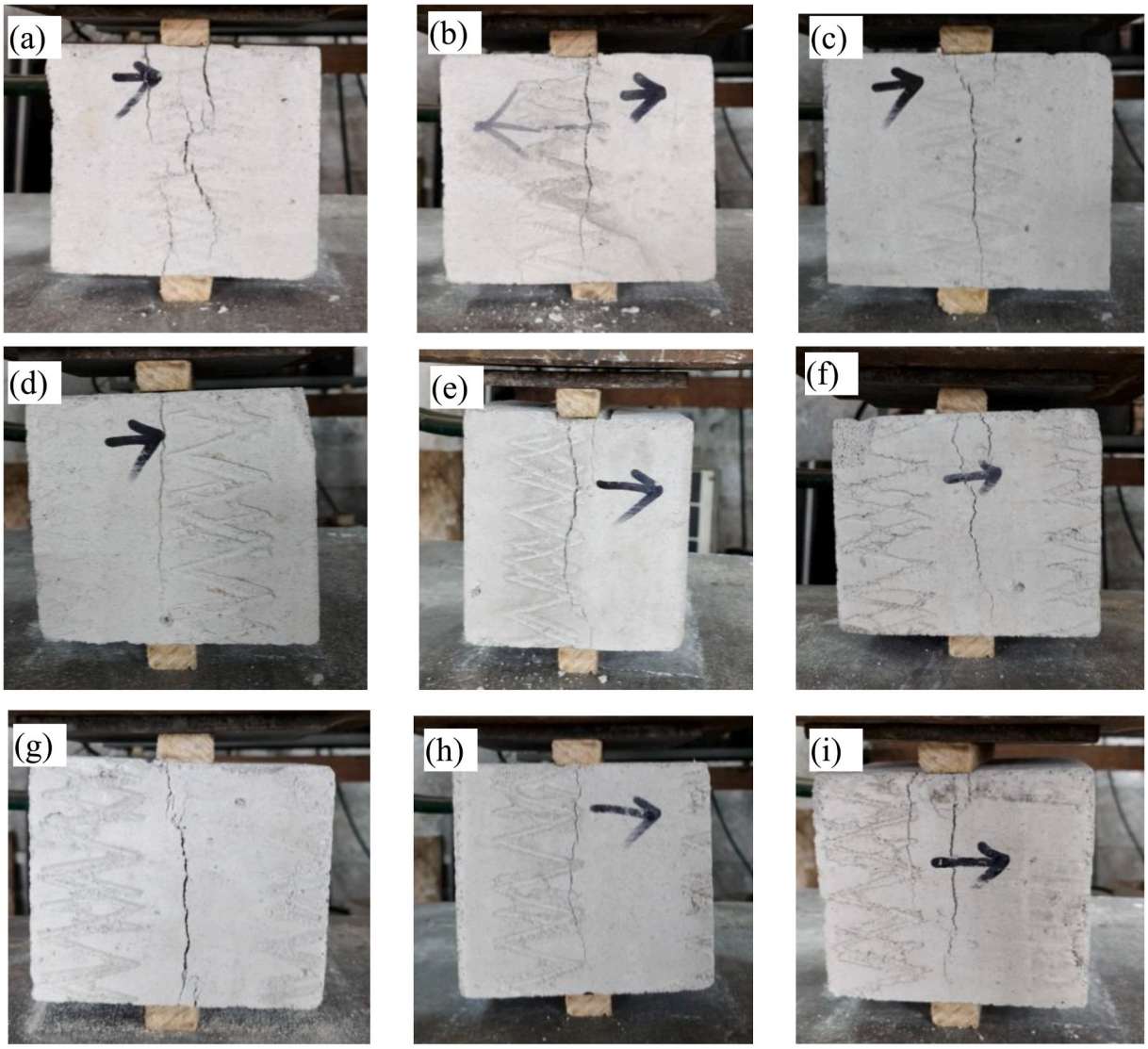

Fig. 9. Various failure/crack patterns observed in AAC cubes under split tensile test.

Table 3
Experimentally obtained mean strength parameters of AAC cubes.

Displacement rate (mm/min)	Strain at peak compressive stress, ε_u	Modulus of Elasticity, E_0 (MPa)	Compressive Strength, σ_{cu} (MPa)	Splitting Tensile Strength, σ_{tu} (MPa)
0.1	0.0136 (0.0094)	123 (36)	1.53 (0.93)	0.39 (0.11)
0.5	0.0201 (0.0113)	206 (39)	2.54 (0.78)	0.45 (0.05)
1.0	0.0169 (0.0132)	258 (58)	2.97 (1.11)	0.46 (0.07)
5.0	0.0098 (0.0030)	409 (135)	3.20 (0.80)	0.54 (0.07)
10.0	0.0098 (0.0047)	479 (151)	3.59 (1.08)	0.59 (0.09)

Note: the values in the parenthesis represent the associated expanded uncertainty.

$$K = \begin{cases} 0.5 \textit{ for compressive strength} \\ 75 \textit{ for elastic modulus} \\ 0.044 \textit{ for splitting tensile strength} \end{cases}$$

Fig. 11 shows the plot between actual (experimentally obtained) and predicted (analytically calculated) compressive strength, elastic modulus, and splitting tensile strength values. It can be seen from these figures that the proposed model predicts the three selected strength properties of the AAC block specimen closely with the experimental results as evidenced from the R^2-values.

Table 4
Comparision of obtained mechanical strength parameters with previous studies.

Reference	Displacement Rate (mm/min)	Mean Compressive Strength (MPa)	Mean Splitting Tensile Strength (MPa)
Present study	0.5	2.54	0.45
Present study	1.0	2.97	0.46
Raj et al. [1]	0.6	2.07	–
Bhosale et al. [2]	1.0	2.95	–
Małyszko et al. [5]	0.5	–	0.34

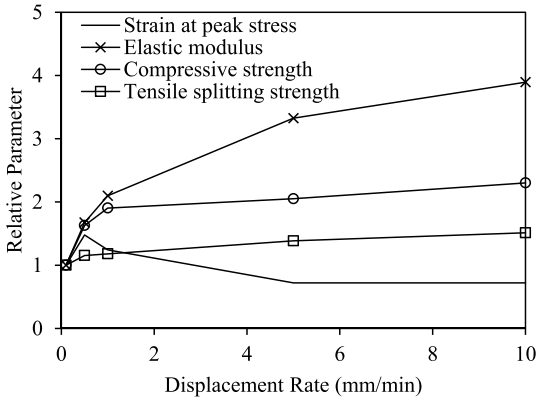

Fig. 10. Variation of mechanical properties of AAC with the displacement rates.

3. Numerical calibration

The described experimental results have been used for the calibration using a commercially available finite element software, Abaqus [16]. The purpose of this section is to understand the internal stress and plastic strain distribution that is generally not possible to visualize through experimental investigation. This model, which treats masonry as an anisotropic continuum and describes its behavior in terms of average stresses and strains, seems an appropriate tool for simulating the behavior of AAC walls. Modified Kent-Park model [46] is used to develop the equivalent backbone curve under compression as follows:

$$\sigma_c = \begin{cases} \sigma_{cu}\left[2\left(\frac{\varepsilon_c}{\varepsilon_u}\right) - \left(\frac{\varepsilon_c}{\varepsilon_u}\right)^2\right]; \varepsilon_c \le \varepsilon_u \\ \sigma_{cu}\left[1 - \left(\frac{(1-\lambda_r)(\varepsilon_c - \varepsilon_u)}{\varepsilon_{20} - \varepsilon_u}\right)^2\right]; \varepsilon_u \le \varepsilon_c \le \varepsilon_{20} \\ \sigma_{cu}\lambda_r; \varepsilon_c \ge \varepsilon_{20} \end{cases} \tag{4}$$

where σ_c and ε_c are the stress and the strain, respectively; σ_{cu} and ε_u are the peak stress and the corresponding strain, respectively. λ_r is the ratio of resident strength to peak stress; and ε_{20} is the strain from which residual strength begins. The mean values of peak stress and the corresponding strain are obtained from the experimental results presented above. Fig. 12 presents a schematic representation of the backbone curve used in the present study.

The finite element analyses were carried out under displacement-controlled loading scheme. The considered material model behavior is initially linear elastic, and then it follows the Concrete Damage Plasticity (CDP) model [47,48] once cracking of the specimen in tension or crushing in compression occurs.

The CDP model used herein uses concepts of isotropic damage in combination with isotropic tensile and compressive plasticity to represent the inelastic behavior of concrete [49,50]. The evolution of the yield surface is controlled by tensile and compressive equivalent plastic strains. The shape of the plasticity surface in the space of High-Westeergard coordinates are presented in Fig. 13. The required plasticity flow parameters are considered from the previous literature [51].

The degradation of the elastic stiffness on the stress-strain curve is characterised by two damage variables for tension and compression, d_t and d_c, which can take any values from zero to one [50]. This response under compression and tension can be depicted as in Fig. 14.

The stress-strain relations under uniaxial tension and compression were taken into account by considering damage variables in Eqs. (5) and (6) [49].

$$\sigma_c = (1 - d_c)E_0\left(\varepsilon_c - \varepsilon_c^{\sim pl}\right) \tag{5}$$

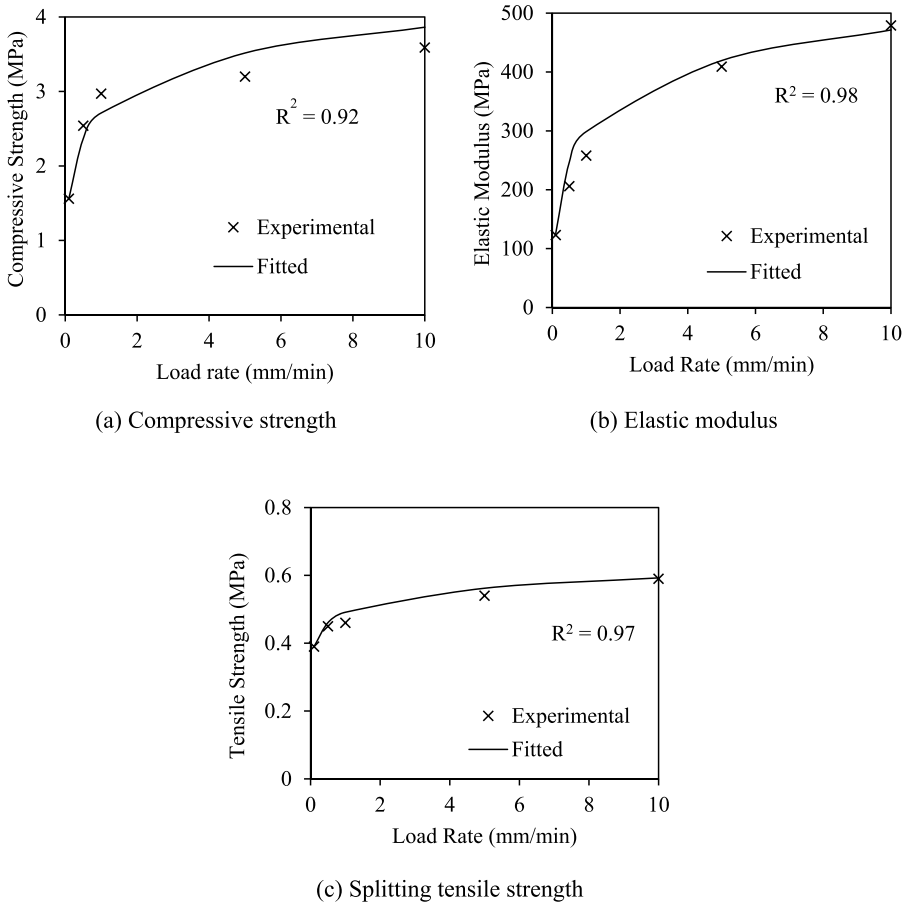

(a) Compressive strength

(b) Elastic modulus

(c) Splitting tensile strength

Fig. 11. Strength parameters predicted by the proposed models.

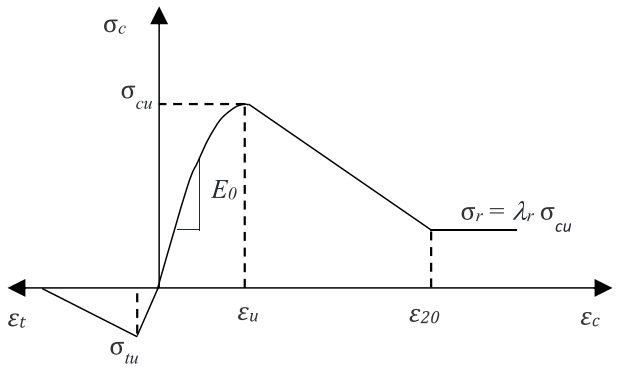

Fig. 12. Stress-strain behavior of concrete under uniaxial compression and tension.

$$\sigma_t = (1 - d_t)E_0\left(\varepsilon_t - \tilde{\varepsilon}_t^{pl}\right) \tag{6}$$

Where, E_0 is the young's modulus, σ_c and σ_t are the compressive and tensile stress, ε_c and ε_t are the compressive and tensile strain. The evolution of the yield (or failure) surface is controlled by two hardening variables, linked to failure mechanisms under tension and compression loading, respectively. We refer to $\tilde{\varepsilon}_c^{pl}$ and $\tilde{\varepsilon}_t^{pl}$ as tensile and compressive equivalent plastic strains, respectively. They can be automatically calculated by Abaqus after the definitions of elastic material behavior.

It is noteworthy that this approach may lead to a slight overestimation of the stiffness of the masonry, but this can be acceptable since the overall behavior in terms of strength and stiffness of the system is significantly influenced by the infills. In addition to the

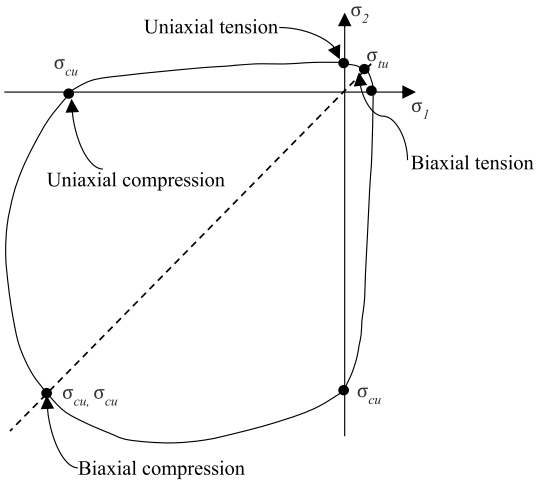

Fig. 13. Biaxial yield surface in CDP Model.

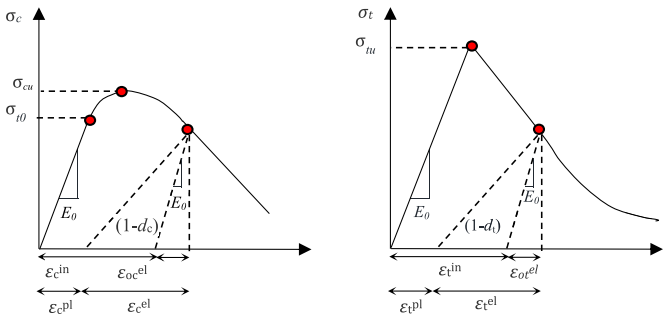

Fig. 14. CDP model both in compression and tension.

mechanical properties presented in Tables 2 and 3, Poisson's ratio of 0.15 is used uniformly to model all the AAC cubes.

In the following sections, the adopted model will be first briefly described and its calibration to the case of AAC masonry will be subsequently discussed. During the modelling strategy, the AAC cube is described with a continuum approach and discretised using 20-noded 3D solid elements.

3.1. Compressive test

It is observed from the experimental tests that for all the selected strain rates, the failure occurs before the displacement of the specimen reaches 2.0 mm that corresponds to a strain of 2.0%. So, to study the relative stress and strain distribution in the AAC specimens under uniaxial compression before and after reaching maximum strain, two limit states; (a) 1.0% and (b) 2.0% strain limits are considered. Fig. 15 and Fig. 16 show the minimum principal stress distribution of AAC cubes loaded with selected strain rates at 1.0% and 2.0% strains respectively.

It can be seen from Figs. 15 and 16 that at a particular level of strain limit, the specimen loaded with a higher strain rate possesses a higher stress concentration casing earlier failure. Similarly, Fig. 17 and Fig. 18 show the plastic strain distributions at 1.0% and 2.0% strain limits, and higher strain concentrations are observed with specimens loaded with higher strain rates. Calibrated numerical outcomes are found to be consistent with the experimental results. The comparison of the experimental and numerical stress-strain distribution of the AAC cube at various loading rates is presented in Fig. 19.

3.2. Tensile test

Numerical models were analysed simulating the tensile test conditions and material parameters and compared with the experimental outcomes. Two limit states (1.5% and 2.5% strain) are selected to describe the relative stress and strain concentrations in the AAC specimens under tension (before and after reaching maximum strain). Fig. 20 and Fig. 21 show the minimum principal stress distribution of AAC cubes loaded with selected strain rates at 1.5% and 2.5% strains respectively. It can be seen from Figs. 20 and 21 that, at a particular level of strain limit, the specimen loaded with a higher strain rate possesses higher as well as nonuniform stress concentrations causing early failure.

Similarly, Fig. 22 and Fig. 23 show the plastic strain distributions at 1.5% and 2.5% strain limits, and higher plastic strain

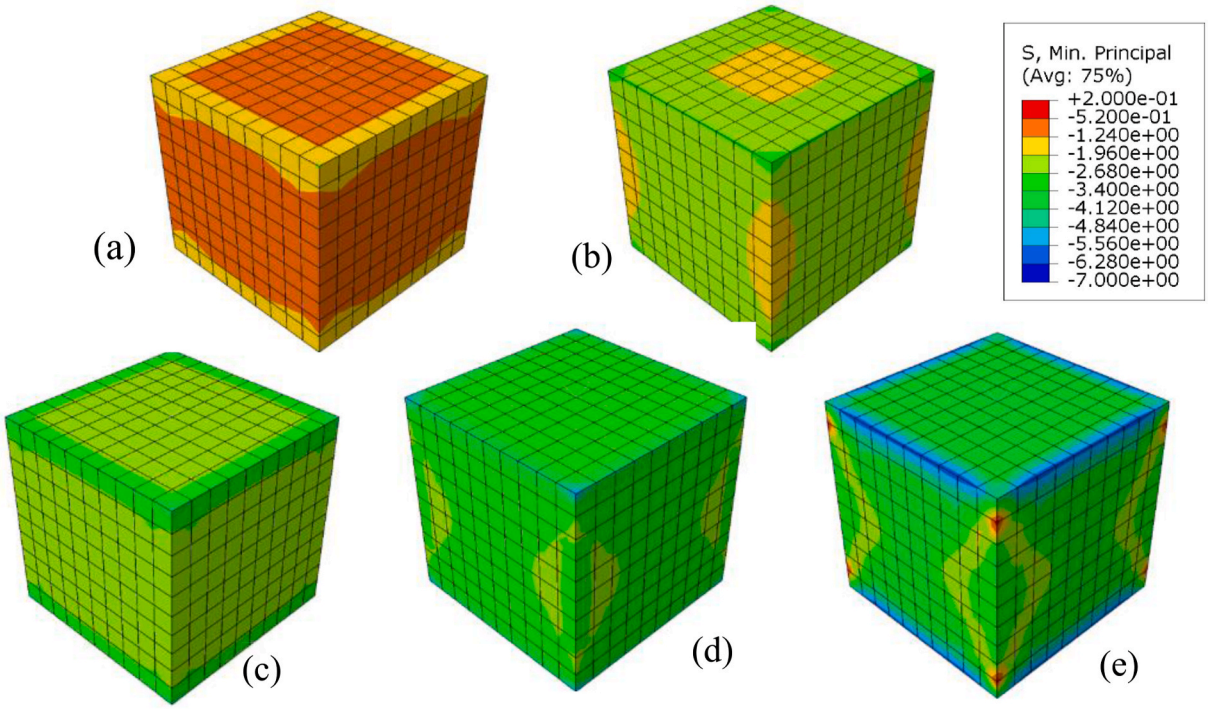

Fig. 15. Distribution of minimum principal stress (in MPa) in AAC cubes at 1% strain for different load rates (a) 0.1(b) 0.5 (c) 1.0 (d) 5.0 (e) 10.0 mm/min.

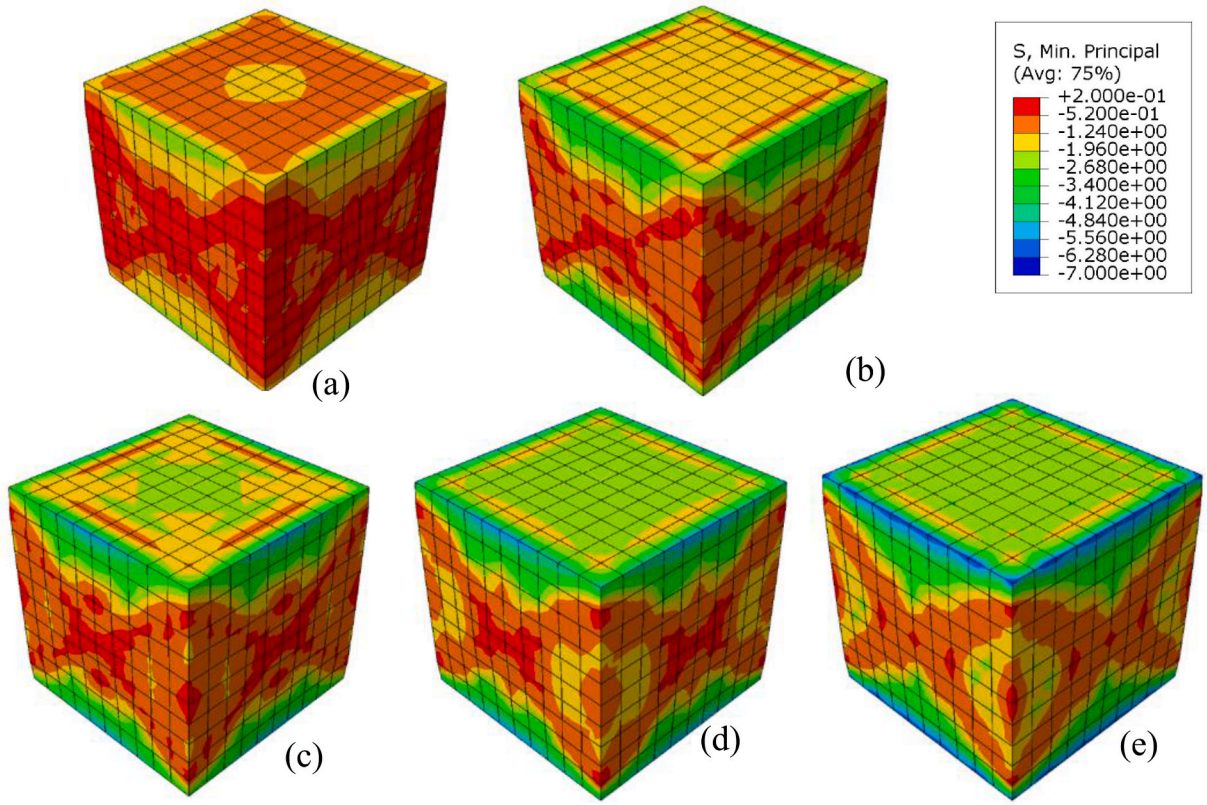

Fig. 16. Distribution of minimum principal stress (in MPa) at 2% strain for different load rates (a) 0.1(b) 0.5 (c) 1.0 (d) 5.0 (e) 10.0 mm/min.

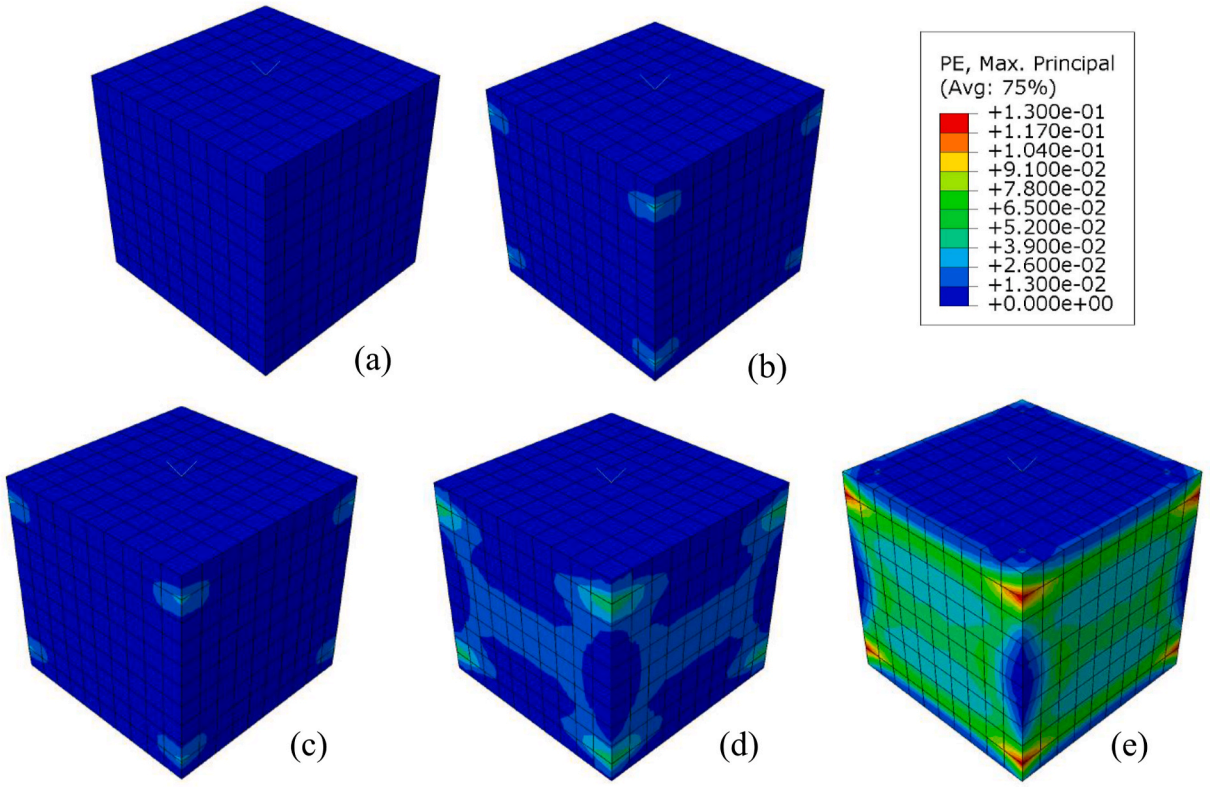

Fig. 17. Distribution of plastic strain at 1% strain for different load rates (a) 0.1 (b) 0.5 (c) 1.0 (d) 5.0 (e) 10.0 mm/min.

concentrations are observed with specimens loaded with higher strain rates. The comparisons of the experimental and numerical stress-strain distribution of the AAC cube at various loading rates are presented in Fig. 24. It can be seen from Table 5 that the FEM calculations are in good agreement with the test results.

4. Summary and conclusions

In this study, an extensive program of systematic laboratory testing has been undertaken to determine the most important mechanical parameters of the AAC masonry subjected to various strain rates. The experimental results showed the significant influence of the strain rates on the compressive, tensile strength, and young's modulus of masonry units. The selected five different levels of strain rates ranged from low to high, scaled with an order of five, shows an increase in the compressive strength, tensile strength, and the modulus of elasticity, and the increase in the strength and elasticity parameter is found to be holding a logarithmic relationship with the strain rates determined statistically.

Although the stress-strain relationship obtained from the experimental outcomes could explain the influence on the mechanical parameters at various selected strain rates, still, some important aspects like, the study of internal principal stress distribution/concentration or plastic strain distribution (showing the failure in the masonry unit) at a selected/particular level of strain was needed to be relatively visualised. So, the experimental outcome is further analysed by a detailed numerical calibration study using a reliable finite element approach. The calibrated numerical models could be able to predict the experimentally obtained stress-strain relationship satisfactorily and the distribution of principal stress and the plastic strain was well visualised and compared. The stress contour shows that at lower strain rates the principal stress is uniformly distributed, whereas with an increasing strain rate the distribution is found to be more irregular. A similar relationship is observed for the plastic strains at various selected strain rates. Along with that, the proposed finite element model appears to be able to correctly catch both the peak load and the experimental crack pattern development, as revealed by the comparison with experimental results.

The experimental test is always found to be expensive as well as time-consuming, whereas numerical modelling can be an efficient way of studying the change in mechanical behavior or doing any parametric study. The proposed modelling approach is more computationally economic and feasible (technological or health reasons) and the mechanical strength parameters in any of the selected strain rates can be predicted using this proposed model. This study is to be further extended to perform the experimental tests on triplets for shear and compression and simulate those experiments in the numerical platform with an efficient modelling approach.

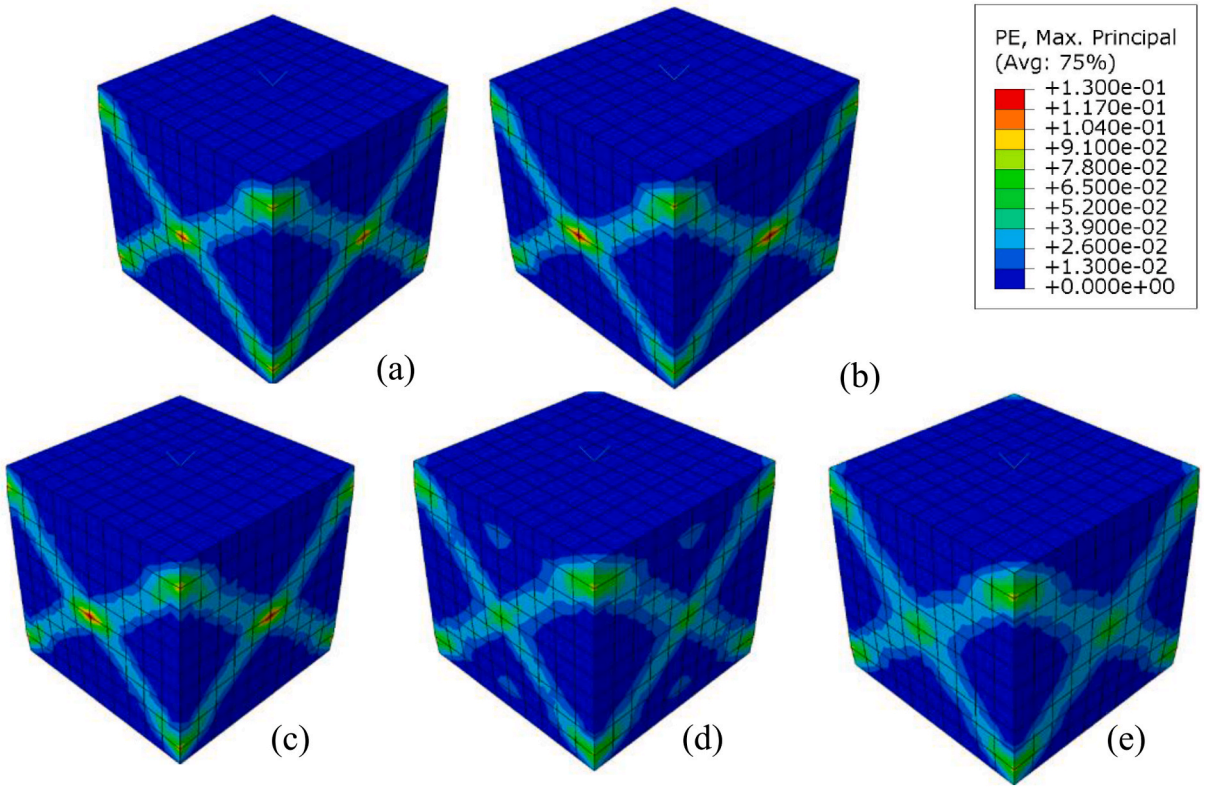

Fig. 18. Distribution of plastic strain at 2% strain for different load rates (a) 0.1 (b) 0.5 (c) 1.0 (d) 5.0 (e) 10.0 mm/min.

CRediT authorship contribution statement

Ningombam Reena Devi: Conceptualization, Methodology, Software, Data curation, Writing- original draft, Visualization, Investigation, Writing – review & editing. **Prateek Kumar Dhir:** Conceptualization, Methodology, Software. **Pradip Sarkar:** Visualization, Investigation, Supervision, Writing – review & editing.

Declaration of competing interest

The authors declare that they have no known competing financial interests or personal relationships that could have appeared to influence the work reported in this paper.

APPENDIX

Table A1
Experimentally obtained strength parameters of AAC cubes

Displacement rate (mm/min)	Samples	Strain at peak comp. stress	Modulus of Elasticity (MPa)	Compressive Strength (MPa)	Splitting Tensile Strength (MPa)
0.1	S1	0.0105	115	1.21	0.42
	S2	0.0101	130	1.24	0.40
	S3	0.0153	117	1.66	0.29
	S4	0.0219	110	2.35	0.36
	S5	0.0129	113	1.25	0.43
	S6	0.0113	155	1.47	0.41
	Mean	0.0136	123	1.53	0.39
	CV	0.33	0.14	0.29	0.14
	U	0.0094	36	0.93	0.11
0.5	S1	0.0223	210	2.63	0.48
	S2	0.0175	202	2.51	0.42
	S3	0.0127	210	2.84	0.45
	S4	0.0246	177	2.47	0.46

(*continued on next page*)

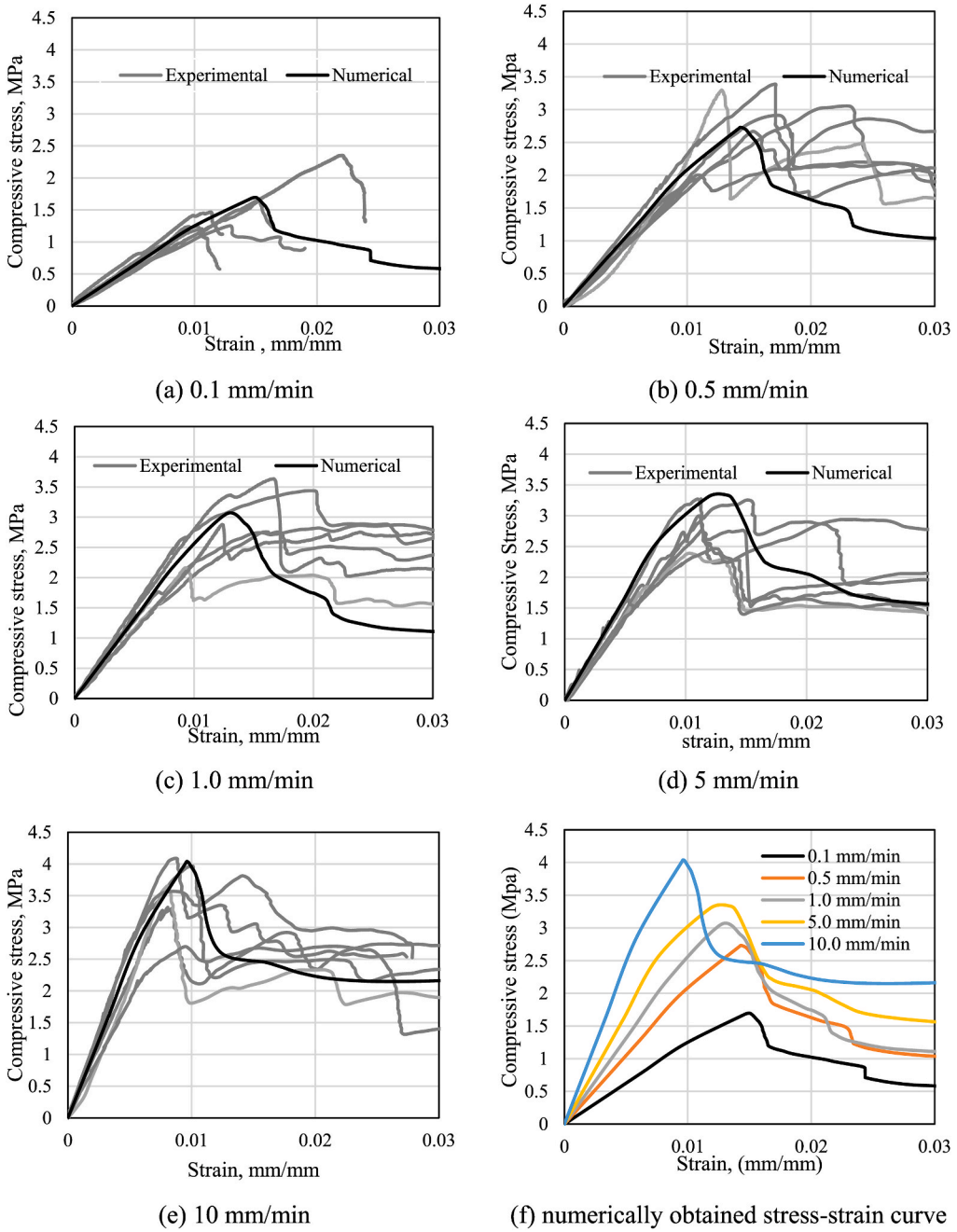

Fig. 19. Comparisons of experimental and numerical responses for AAC cubes under monotonic compression at various load rates.

Table A1 (*continued*)

Displacement rate (mm/min)	Samples	Strain at peak comp. stress	Modulus of Elasticity (MPa)	Compressive Strength (MPa)	Splitting Tensile Strength (MPa)
	S5	0.0269	203	1.88	0.46
	S6	0.0171	234	2.92	0.42
	Mean	0.0201	206	2.54	0.45
	CV	0.26	0.09	0.15	0.05
	U	0.0113	39	0.78	0.05
1.0	S1	0.0273	258	2.87	0.45
	S2	0.0166	277	3.64	0.44
	S3	0.0162	223	2.78	0.44

(*continued on next page*)

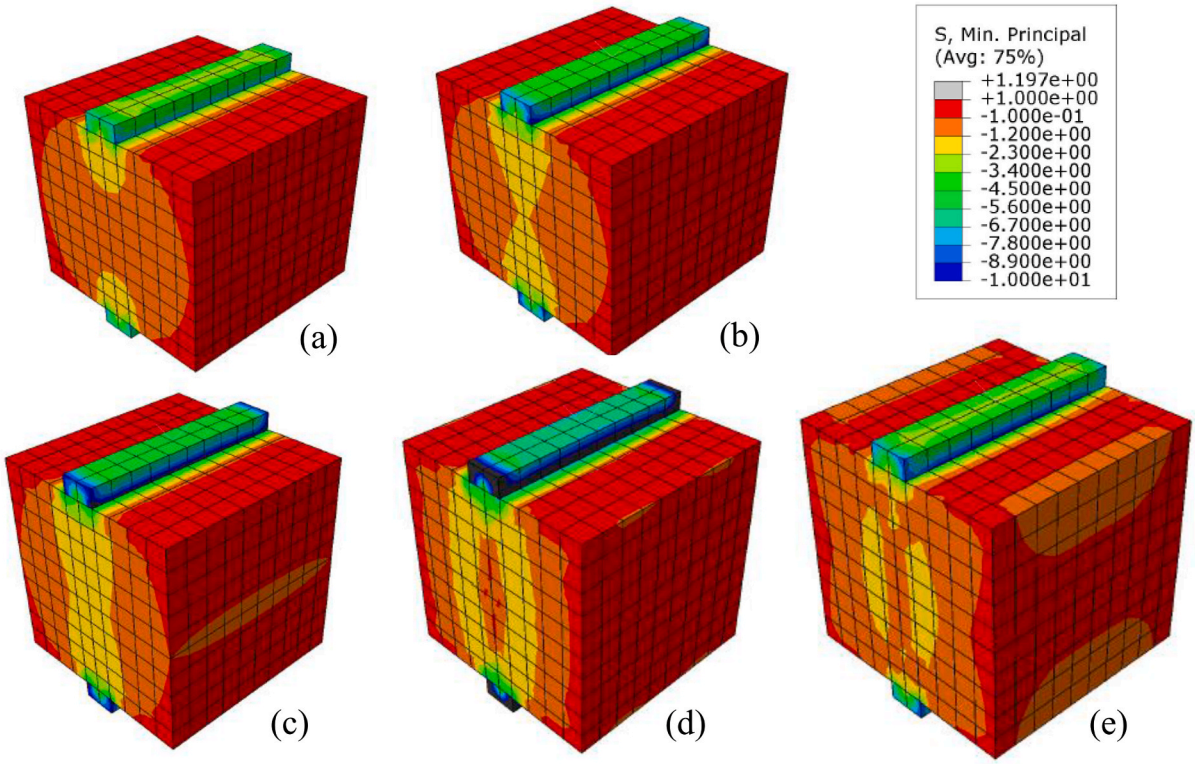

Fig. 20. Distribution of minimum principal stress (MPa) at 1.5% strain for different load rates (a) 0.1 (b) 0.5 (c) 1.0 (d) 5.0 (e) 10.0 mm/min.

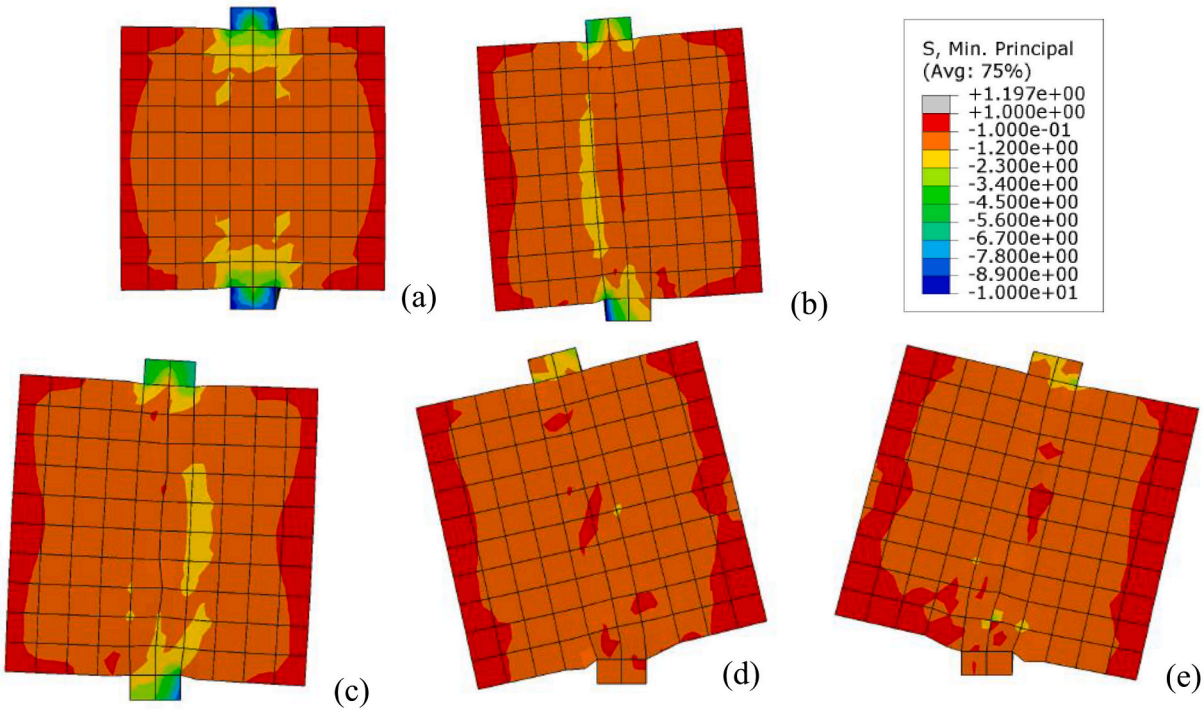

Fig. 21. Distribution of minimum principal stress (MPa) at 2.5% strain for different load rates (a) 0.1 (b) 0.5 (c) 1.0 (d) 5.0 (e) 10.0 mm/min.

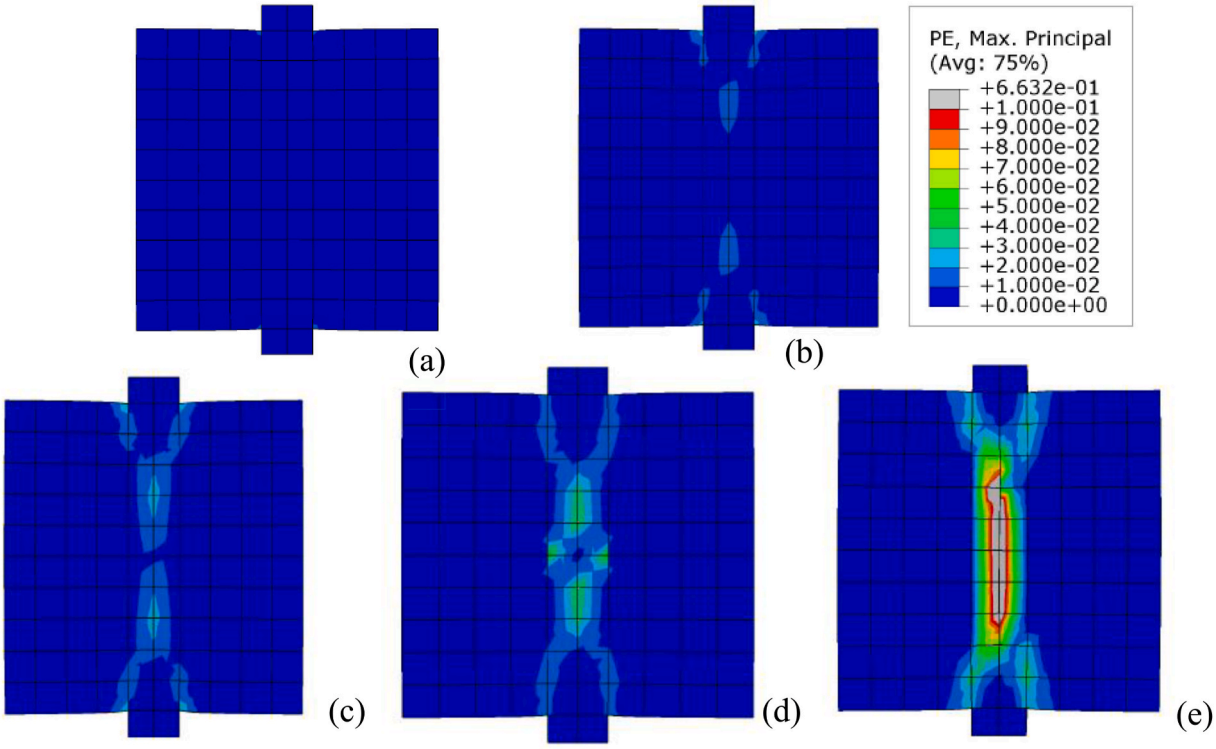

Fig. 22. Distribution of plastic strain at 1.5% strain for different load rates (a) 0.1 (b) 0.5 (c) 1.0 (d) 5.0 (e) 10.0 mm/min.

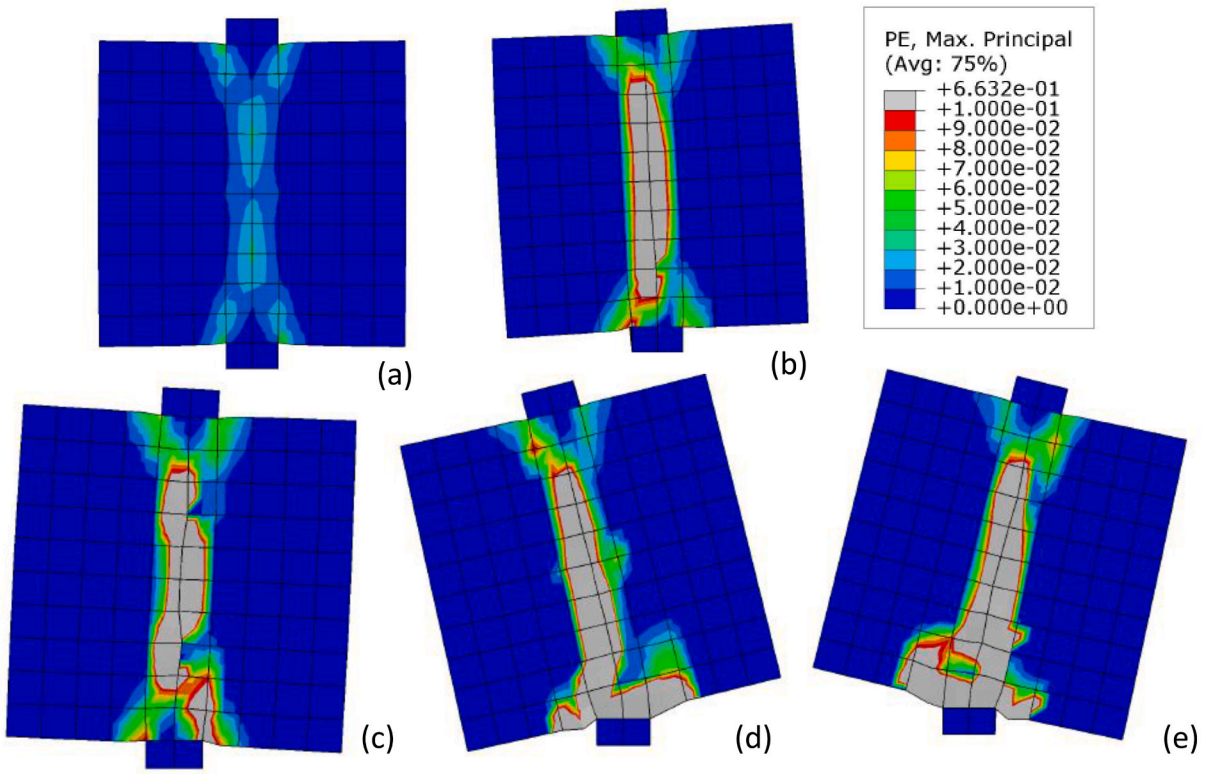

Fig. 23. Distribution of plastic strain at 2.5% strain for different load rates (a) 0.1 (b) 0.5 (c) 1.0 (d) 5.0 (e) 10.0 mm/min.

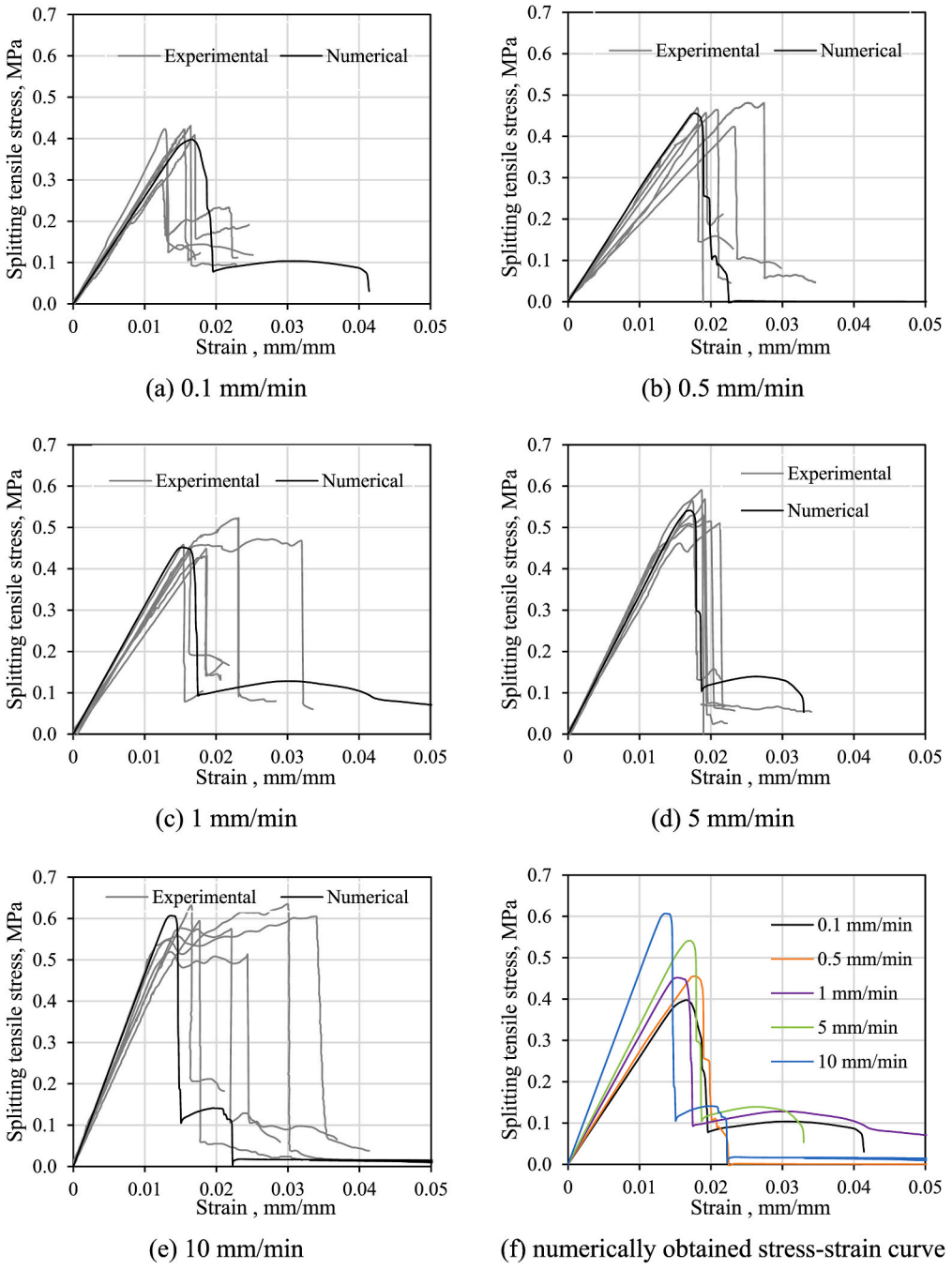

Fig. 24. Comparisons of Experimental and Numerical responses for AAC cubes under tensile loading at various rates of loadings.

Table A1 (*continued*)

Displacement rate (mm/min)	Samples	Strain at peak comp. stress	Modulus of Elasticity (MPa)	Compressive Strength (MPa)	Splitting Tensile Strength (MPa)
	S4	0.0092	259	2.17	0.43
	S5	0.0197	298	3.45	0.52
	S6	0.0123	234	2.88	0.47
	Mean	0.0169	258	2.97	0.46
	CV	0.37	0.11	0.18	0.07
	U	0.0132	58	1.11	0.07

(*continued on next page*)

Table 5
Comparison between FEM calculations and test results.

Parameters		Displacement rate (mm/min)				
		0.1	0.5	1.0	5.0	10.0
E_0 (MPa)	Experimental	123	206	258	409	479
	FEA	125	210	263	415	488
	Deviation (%)	1.63	1.94	1.94	1.47	1.88
σ_{cu} (MPa)	Experimental	1.53	2.54	2.97	3.20	3.59
	FEA	1.61	2.63	3.08	3.35	3.87
	Deviation (%)	5.23	3.54	3.70	4.69	7.80
σ_{tu} (MPa)	Experimental	0.39	0.45	0.46	0.54	0.59
	FEA	0.40	0.46	0.47	0.55	0.60
	Deviation (%)	2.56	2.22	2.17	1.85	1.69

Table A1 (*continued*)

Displacement rate (mm/min)	Samples	Strain at peak comp. stress	Modulus of Elasticity (MPa)	Compressive Strength (MPa)	Splitting Tensile Strength (MPa)
5.0	S1	0.0092	348	3.40	0.58
	S2	0.0094	380	3.20	0.56
	S3	0.0085	387	2.75	0.51
	S4	0.0125	528	3.28	0.50
	S5	0.0102	381	2.83	0.52
	S6	0.0094	430	3.77	0.56
	Mean	0.0098	409	3.20	0.54
	CV	0.14	0.16	0.12	0.06
	U	0.0030	135	0.80	0.07
10.0	S1	0.0100	547	3.96	0.51
	S2	0.0084	423	3.32	0.59
	S3	0.0081	466	3.67	0.63
	S4	0.0095	371	2.70	0.57
	S5	0.0141	544	3.82	0.60
	S6	0.0088	520	4.09	0.63
	Mean	0.0098	479	3.59	0.59
	CV	0.23	0.15	0.14	0.08
	U	0.0047	151	1.08	0.09

CV represents the coefficient of variation while *U* represents the expanded uncertainty.

References

[1] A. Raj, A.C. Borsaikia, U.S. Dixit, Bond strength of Autoclaved Aerated Concrete (AAC) masonry using various joint materials, J. Build. Eng. 28 (2020), 101039.
[2] A. Bhosale, N.P. Zade, R. Davis, P. Sarkar, Experimental investigation of autoclaved aerated concrete masonry, J. Mater. Civ. Eng. 31 (7) (2019), 04019109.
[3] G. Pachideh, M. Gholhaki, Effect of pozzolanic materials on mechanical properties and water absorption of autoclaved aerated concrete, J. Build. Eng. 26 (2019), 100856.
[4] F. Seddighi, G. Pachideh, S.B. Salimbahrami, A study of mechanical and microstructures properties of autoclaved aerated concrete containing nano-graphene, J. Build. Eng. 43 (2021), 103106.
[5] L. Małyszko, E. Kowalska, P. Bilko, Splitting tensile behavior of autoclaved aerated concrete: comparison of different specimens' results, Construct. Build. Mater. 157 (2017) 1190–1198.
[6] S. Harsh, Z. Shen, D. Darwin, Strain-Rate Sensitive Behavior of Cemet Paste and Mortar in Compression, American Concrete Institute, 1990.
[7] J.F. Wang, X. Wu, X.L. Fan, Y.R. Chen, Stress–strain model of cement asphalt mortar subjected to temperature and loading rate, Construct. Build. Mater. 111 (2016) 164–174.
[8] W. Yao, K. Xia, Y. Liu, Y. Shi, K. Peterson, Dependences of dynamic compressive and tensile strengths of four alkali-activated mortars on the loading rate and curing time, Construct. Build. Mater. 202 (2019) 891–903.
[9] H. Hao, B.G. Tarasov, Experimental study of dynamic material properties of clay brick and mortar at different strain rates, Aust. J. Struct. Eng. 8 (2) (2008) 117–132.
[10] X. Wei, H. Hao, Numerical derivation of homogenised dynamic masonry material properties with strain rate effects, Int. J. Impact Eng. 36 (3) (2009) 522–536.
[11] A.N. Stavrogin, B.G. Tarasov (Eds.), Experimental Physics and Rock Mechanics, CRC Press, 2001.
[12] K.N. Feng, D. Ruan, Z. Pan, F. Collins, Y. Bai, C.M. Wang, W.H. Duan, Mechanical behavior of geopolymer concrete subjected to high strain rate compressive loadings, Mater. Struct. 48 (3) (2015) 671–681.
[13] M. Khandelwal, P.G. Ranjith, Z. Pan, J.G. Sanjayan, Effect of strain rate on strength properties of low-calcium fly-ash-based geopolymer mortar under dry condition, Arabian J. Geosci. 6 (7) (2013) 2383–2389.
[14] P.G. Ranjith, D. Jasinge, J.Y. Song, S.K. Choi, A study of the effect of displacement rate and moisture content on the mechanical properties of concrete: use of acoustic emission, Mech. Mater. 40 (6) (2008) 453–469.
[15] H. Hao, X.Q. Zhou, Concrete material model for high rate dynamic analysis, in: Proceedings, 2007, October, pp. 753–768.
[16] Abaqus, Dassault Systemes, 2020. https://www.3ds.com/products-services/simulia/products/abaqus/abaquscae/.
[17] A. Bhosale, N.P. Zade, P. Sarkar, R. Davis, Mechanical and physical properties of cellular lightweight concrete block masonry, Construct. Build. Mater. 248 (2020), 118621.
[18] S. Barattucci, V. Sarhosis, A.W. Bruno, A.M. D'Altri, S. de Miranda, G. Castellazzi, An experimental and numerical study on masonry triplets subjected to monotonic and cyclic shear loadings, Construct. Build. Mater. 254 (2020), 119313.
[19] H.B. Kaushik, D.C. Rai, S.K. Jain, Stress-strain characteristics of clay brick masonry under uniaxial compression, J. Mater. Civ. Eng. 19 (9) (2007) 728–739.

[20] J.M.L. Reis, A.R. Carvalho, H.S. da Costa Mattos, Effects of displacement rate and temperature on the fracture properties of polymer mortars, Construct. Build. Mater. 55 (2014) 1–4.
[21] J.F. Wang, Y.R. Chen, X.L. Fan, J.Z. Li, Effects of strain rate and confining pressure on compressive behavior of cement asphalt mortar, Mater. Des. 65 (2015) 772–779, 1980-2015.
[22] X. Zhang, L. Garijo, G. Ruiz, J.J. Ortega, Loading-rate effect on the fracture response of natural hydraulic and aerial-lime mortars, J. Mater. Civ. Eng. 32 (9) (2020), 04020258.
[23] S. Tandon, K.T. Faber, Effects of loading rate on the fracture of cementitious materials, Cement Concr. Res. 29 (3) (1999) 397–406.
[24] B.H. Oh, Fracture behavior of concrete under high rates of loading, Eng. Fract. Mech. 35 (1–3) (1990) 327–332.
[25] Is: 2185-3, Concrete Masonry Units, Part 3: Autoclaved Cellular Aerated Concrete Blocks [CED 53: Cement Matrix Products, Bureau of Indian Standards., New Delhi, India, 1984.
[26] Astm, C., 2017. vols. 1693–11, Standard Specification for Autoclaved Aerated Concrete (AAC). American Society for Testing and Materials, Philadelphia, PA.
[27] Astm, C., 2012. vols. 67–12, Standard Test Methods for Sampling and Testing Brick and Structural Clay Tile. American Society for Testing and Materials, Philadelphia, PA.
[28] F. Pospisil, J. Jambor, J. Belko, Unit Weight Reduction of Fly Ash Aerated Concrete, Rotterdam, Netherland:. Advances in Autoclaved Aerated Concrete, AA Balkema, 1992, pp. 43–52.
[29] I. Odler, M. Rößler, Investigations on the relationship between porosity, structure and strength of hydrated Portland cement pastes. II. Effect of pore structure and of degree of hydration, Cement Concr. Res. 15 (3) (1985) 401–410.
[30] K. Hanečka, O.G. Koronthályová, P.M. Mšovský, The carbonation of autoclaved aerated concrete, Cement Concr. Res. 27 (4) (1997) 589–599.
[31] N. Narayanan, K. Ramamurthy, Structure and properties of aerated concrete: a review, Cement Concr. Compos. 22 (5) (2000) 321–329.
[32] N. Isu, H. Ishida, T. Mitsuda, Influence of quartz particle size on the chemical and mechanical properties of autoclaved aerated concrete (I) tobermorite formation, Cement Concr. Res. 25 (2) (1995) 243–248.
[33] N. Isu, S. Teramura, H. Ishida, T. Mitsuda, Influence of quartz particle size on the chemical and mechanical properties of autoclaved aerated concrete (II) fracture toughness, strength and micropore, Cement Concr. Res. 25 (2) (1995) 249–254.
[34] RILEM, Autoclaved Aerated Concrete: Properties, Testing and Design, Taylor & Francis, London, 1993.
[35] R. Jasiński, Ł. Drobiec, W. Mazur, Validation of selected non-destructive methods for determining the compressive strength of masonry units made of autoclaved aerated concrete, Materials 12 (3) (2019) 389.
[36] R. Jasiński, Identification of stress states in compressed masonry walls using a non-destructive technique (NDT), Materials 13 (12) (2020) 2852.
[37] R. Jasiński, K. Stebel, P. Kielan, Use of the AE effect to determine the stresses state in AAC masonry walls under compression, Materials 14 (13) (2021) 3459.
[38] S. Mallikarjuna, Experimental Determination of Parameters for a Micro-modeling Based Failure Criterion for AAC Block Masonry Shear Wall, MTech thesis, Indian Institute of Technology, Guwahati, India, 2017.
[39] A.A. Costa, A. Penna, G. Magenes, A. Galasco, Seismic performance assessment of autoclaved aerated concrete (AAC) masonry buildings, in: Proc. The 14th World Conference on Earthquake Engineering, 2008, October, pp. 12–17.
[40] B.S. EN, Testing Hardened Concrete–Part 3: Compressive Strength of Test Specimens, British Standard Institution, London, UK, 2009.
[41] Z. Jinping, C. Jianxing, C. Xuefeng, Q. Hao, Experiment research of concrete splitting tensile strength based on age and curing temperature, in: In IOP Conference Series: Earth and Environmental Science, vol. 267, IOP Publishing, 2019, May, 052056, 5.
[42] G.J. Hahn, R.W. Hendrickson, A table of percentage points of the distribution of the largest absolute value of k Student t variates and its applications, Biometrika 58 (2) (1971) 323–332.
[43] IS:8900, Criteria for the Rejection of Outlying Observations, Bureau of Indian Standards., New Delhi, India, 1978.
[44] C. Qi, M. Wang, Q. Qian, Strain-rate effects on the strength and fragmentation size of rocks, Int. J. Impact Eng. 36 (12) (2009) 1355–1364.
[45] Y.U. Shui-Sheng, L.U. Yu-Bin, C.A.I. Yong, The strain-rate effect of engineering materials and its unified model, Lat. Am. J. Solid. Struct. 10 (4) (2013) 833–844.
[46] B.D. Scott, R. Park, M.J. Priestley, Stress-strain behavior of concrete confined by overlapping hoops at low and high strain rates, Int. J. Proc. 79 (1) (1982, January) 13–27.
[47] J. Lee, G.L. Fenves, A plastic-damage concrete model for earthquake analysis of dams, Earthq. Eng. Struct. Dynam. 27 (9) (1998) 937–956.
[48] Concrete damaged plasticity, Abaqus manual, 2017. https://abaqus479docs.mit.edu/2017/English/SIMACAEMATRefMap/simamat-c-concretedamaged.htm.
[49] J. Lubliner, J. Oliver, S. Oller, E. Oñate, A plastic-damage model for concrete, Int. J. Solid Struct. 25 (3) (1989) 299–326.
[50] J. Lee, G.L. Fenves, Plastic-damage model for cyclic loading of concrete structures, J. Eng. Mech. 124 (8) (1998) 892–900.
[51] T. Yu, J.G. Teng, Y.L. Wong, S.L. Dong, Finite element modeling of confined concrete-II: plastic-damage model, Eng. Struct. 32 (3) (2010) 680–691.